AGU PUBLICATIONS

JGR

Journal of Geophysical Research: Atmospheres

RESEARCH ARTICLE
10.1002/2015JD023929

Spatiotemporal drought variability in the Mediterranean over the last 900 years

Benjamin I. Cook[1,2], Kevin J. Anchukaitis[3,4,5], Ramzi Touchan[4], David M. Meko[4], and Edward R. Cook[5]

[1]NASA Goddard Institute for Space Studies, New York, New York, USA, [2]Ocean and Climate Physics, Lamont-Doherty Earth Observatory, Palisades, New York, USA, [3]School of Geography and Development, University of Arizona, Tucson, Arizona, USA, [4]Laboratory of Tree-Ring Research, University of Arizona, Tucson, Arizona, USA, [5]Tree Ring Laboratory, Lamont-Doherty Earth Observatory, Palisades, New York, USA

Key Points:
- There is large multidecadal drought variability across the Mediterranean over the last 900 years
- Droughts tend to be zonally symmetric, but there is strong north-south antiphasing in eastern basin
- There is an 89%/98% likelihood that the recent Levant drought is the worst of the last 900/500 years

Correspondence to:
B. I. Cook,
benjamin.i.cook@nasa.gov

Citation:
Cook, B. I., K. J. Anchukaitis, R. Touchan, D. M. Meko, and E. R. Cook (2016), Spatiotemporal drought variability in the Mediterranean over the last 900 years, *J. Geophys. Res. Atmos.*, *121*, 2060–2074, doi:10.1002/2015JD023929.

Received 13 JUL 2015
Accepted 30 JAN 2016
Accepted article online 4 FEB 2016
Published online 4 MAR 2016

Abstract Recent Mediterranean droughts have highlighted concerns that climate change may be contributing to observed drying trends, but natural climate variability in the region is still poorly understood. We analyze 900 years (1100–2012) of Mediterranean drought variability in the Old World Drought Atlas (OWDA), a spatiotemporal tree ring reconstruction of the June-July-August self-calibrating Palmer Drought Severity Index. In the Mediterranean, the OWDA is highly correlated with spring precipitation (April–June), the North Atlantic Oscillation (January–April), the Scandinavian Pattern (January–March), and the East Atlantic Pattern (April–June). Drought variability displays significant east-west coherence across the basin on multidecadal to centennial timescales and north-south antiphasing in the eastern Mediterranean, with a tendency for wet anomalies in the Black Sea region (e.g., Greece, Anatolia, and the Balkans) when coastal Libya, the southern Levant, and the Middle East are dry, possibly related to the North Atlantic Oscillation. Recent droughts are centered in the western Mediterranean, Greece, and the Levant. Events of similar magnitude in the western Mediterranean and Greece occur in the OWDA, but the recent 15 year drought in the Levant (1998–2012) is the driest in the record. Estimating uncertainties using a resampling approach, we conclude that there is an 89% likelihood that this drought is drier than any comparable period of the last 900 years and a 98% likelihood that it is drier than the last 500 years. These results confirm the exceptional nature of this drought relative to natural variability in recent centuries, consistent with studies that have found evidence for anthropogenically forced drying in the region.

1. Introduction

Climate change impacts on water resources are a significant concern in the regions surrounding the Mediterranean Sea [*Iglesias et al.*, 2007; *García-Ruiz et al.*, 2011], an area including southern Europe, northern Africa, and the Levant region of the Middle East (Cyprus, Israel, Jordan, Lebanon, Palestine, Syria, and Turkey). Projections from climate models almost uniformly point toward drying in the Mediterranean from increased greenhouse gas forcing in the coming decades [*Giorgi and Lionello*, 2008; *Collins et al.*, 2013; *Seager et al.*, 2014], part of an overall trend toward desiccation and poleward expansion of subtropical dry zones [*Held and Soden*, 2006; *Seager et al.*, 2010]. Indeed, analyses of recent climate trends in the region suggest that this process may have already begun [*García-Ruiz et al.*, 2011; *Gleick*, 2014; *Hoerling et al.*, 2012; *Kelley et al.*, 2012, 2015].

However, a more complete understanding of natural Mediterranean drought variability and anthropogenically forced moisture trends requires comparisons with long-term variability that is not available from relatively short instrumental records. To this end, the paleoclimate community has been active throughout this region, developing estimates of Common Era drought variability from a variety of proxies, including tree rings [*Brewer et al.*, 2007; *Chbouki et al.*, 1995; *Glueck and Stockton*, 2001; *Touchan et al.*, 2003; *Akkemik and Aras*, 2005; *Touchan et al.*, 2005; *Esper et al.*, 2007; *Andreu et al.*, 2007; *Nicault et al.*, 2008; *Touchan et al.*, 2008a; *Büntgen et al.*, 2010; *Touchan et al.*, 2011; *Köse et al.*, 2011; *Touchan et al.*, 2014a], sediment cores [e.g., *Jones et al.*, 2006; *Roberts et al.*, 2012; *Moreno et al.*, 2012], speleothems [e.g., *Jex et al.*, 2011; *Wassenburg et al.*, 2013], and networks using multiple proxies [*Carro-Calvo et al.*, 2013; *Luterbacher et al.*, 2012; *Pauling et al.*, 2006]. To date, however, there is little consensus across these different records regarding the character and dominant

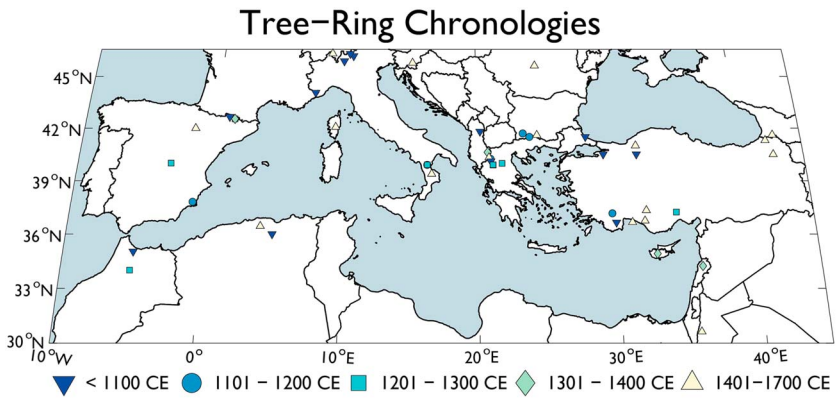

Figure 1. Locations of tree ring chronologies in the Mediterranean region of the Old World Drought Atlas. Colors and marker shapes indicate the approximate start dates of the various chronologies.

drivers of drought variability across the basin over the last millennium. In particular, there are extant uncertainties regarding how widespread droughts are in the Mediterranean [*Roberts et al.*, 2012], the magnitude and timing of long-term trends and centennial-scale variability [*Esper et al.*, 2007; *Touchan et al.*, 2011; *Wassenburg et al.*, 2013], and how seasonal signals and large-scale climate modes are reflected in proxy reconstructions [*Touchan et al.*, 2014a, 2014b; *Seim et al.*, 2015].

Given these uncertainties, the development and analysis of new large-scale reconstructions is imperative for improving our understanding of climate dynamics in the Mediterranean. Here we use a spatially resolved tree ring-based field reconstruction of European and Mediterranean hydroclimate to investigate the dominant spatiotemporal patterns of drought variability across the basin over nearly the entirety of the last millennium. Specifically, our analysis addresses three primary research questions: (1) What are the dominant modes of hydroclimate variability in the Mediterranean? (2) How spatially coherent are drought events across the Mediterranean Basin? (3) And how do recent droughts compare to long-term hydroclimate variability over the last 900 years?

2. Materials and Methods

2.1. The Old World Drought Atlas

The Old World Drought Atlas (OWDA) [*Cook et al.*, 2015] is a new, tree ring-based reconstruction of summer season (June-July-August, JJA) self-calibrating Palmer Drought Severity Index (scPDSI) [*van der Schrier et al.*, 2013]. The OWDA uses 106 tree ring chronologies to reconstruct scPDSI at 5414 half-degree grid points for the entire Common Era over the European-Mediterranean domain (27°N–71°N, 12°W–45°E). The reconstruction uses the point-by-point method [*Cook et al.*, 1999, 2013] with a proxy search radius of 1000 km around each target grid point. Grid cell scPDSI is reconstructed from the proxy predictor series within the search radius, but the tree ring proxies are effectively weighted by the principal components regression such that those that covary most strongly with observations have the greatest influence on the reconstructions. Proxy site locations in the Mediterranean portion of the OWDA (30°N–47°N, 10°W–45°E) are shown in Figure 1, along with the approximate start dates of the various records.

The longest available chronologies (start year before 1100 or 1200 C.E.) are well distributed across the Mediterranean region, with greatest densities in Anatolia, the western Mediterranean, and Northern Italy. For regions where these longer chronologies are not available locally (e.g., the Levant and Middle East) the 1000 km search radius (roughly equivalent to the correlation decay *e*-folding distance of the PDSI being reconstructed; see the Supplemental Materials in *Cook et al.* [2015]) allows for reconstructions further back in time than the shorter local chronologies would allow. For example, the longest pre-1100 C.E. chronologies from Anatolia are within 1000 km of the Levant and Middle East region and used in the OWDA to reconstruct scPDSI in these regions prior to the start date of the local chronologies, which mostly begin in the 1300s and 1400s. In such cases, the grid point reconstruction is still required to pass minimum calibration and validation thresholds to be included in the drought atlas. Up to 1978, scPDSI values in the OWDA are from the tree ring reconstruction, which are merged with the instrumental data from 1979 to 2012. Complete details on

the OWDA calibration and validation can be found in the Supplemental Materials of *Cook et al.* [2015]. Given these caveats, we therefore have confidence that the temporal coverage (1100–2012 C.E.) and spatial domain of our analyses are well supported.

The scPDSI itself is a modification of the original PDSI formulation of *Palmer* [1965], a locally normalized drought index incorporating changes in supply (precipitation), demand (evapotranspiration), and storage (soil moisture). PDSI has an inherent memory timescale of 12–18 months [*Guttman*, 1998; *Vicente-Serrano et al.*, 2010], allowing the JJA target of the OWDA to incorporate climate information from the previous winter and spring, the main seasons of moisture supply to the Mediterranean [*Touchan et al.*, 2011]. The scPDSI used as the target for the OWDA reconstruction [*van der Schrier et al.*, 2013] is calculated from version TS3.21 of the high-resolution Climatic Research Unit (CRU) climate grids [*Harris et al.*, 2014], incorporates a snow module, and uses the Penman-Monteith formulation for calculating potential evapotranspiration [*Xu and Singh*, 2002].

2.2. Climate Data

Monthly precipitation data are from the high-resolution CRU gridded climate data (TS3.21) [*Harris et al.*, 2014]. We also use monthly average climate indices from the Climate Prediction Center for modes that have been previously shown to have an influence on Mediterranean climate [*Sousa et al.*, 2011]. The North Atlantic Oscillation (NAO) [*Hurrell*, 1995] consists of a north-south dipole in atmospheric pressure between Greenland and the subtropical North Atlantic, with positive phases typically associated with below-average precipitation in the Mediterranean and southern Europe. The Scandinavian Pattern (SCA) [*Bueh and Nakamura*, 2007] is centered over Scandinavia, with positive height anomalies in this region causing above-average precipitation across central and southern Europe. The East Atlantic Pattern (EA) [*Barnston and Livezey*, 1987] is similar to the NAO, consisting of a north-south anomaly dipole in the Atlantic. Unlike the NAO, however, the EA has stronger connections to the subtropical ridge. Positive phases of the EA are linked to below-average precipitation across southern Europe. For the CRU precipitation data and the climate indices, we restrict our analysis for the most recent period when data quality and availability is highest (1950–2012).

2.3. Analyses

To account for the loss of grid cells with declining proxy availability (and regression model degradation) in the past, we use a frozen grid. Any missing grid cells in year 1100 C.E. (the first year of our analysis) were treated as missing in all subsequent years. This ensures stationarity in the number of observations available in all years of our analysis.

We use Spearman's rank correlations to assess the statistical relationship between reconstructions, observations, and indices. Spearman's is a nonparametric alternative to the Pearson product-moment correlation that is less sensitive to outliers. In all correlation plots, regions with insignificant correlations ($p > 0.05$) are masked by grey asterisks. For regional time series, uncertainties are estimated as the 95th percentile bias-corrected and accelerated (BCa) [*Efron*, 1987] bootstrap confidence intervals. On the relevant figures, these confidence intervals are shown by the grey-blue shading around the time series. In some figures, the time series were smoothed using a 10 year loess fit [*Cleveland and Devlin*, 1988] to emphasize low-frequency variability, although all statistical analyses were conducted on the original (unsmoothed) data.

Spectral and spectral coherency analyses are conducted in two ways. The first is a multitaper approach [*Thomson*, 1982; *Chave et al.*, 1987; *Mann and Lees*, 1996; *Czaja and Marshall*, 2001; *Huybers*, 2004] with significance levels estimated using a nonparametric Monte Carlo procedure with red noise (AR1) conditioned on the original data. We also use wavelet coherency analyses [*Maraun and Kurths*, 2004; *Maraun et al.*, 2007] to investigate time-varying coherency and phasing between various drought series. Following the best practice recommendations in *Grinsted et al.* [2004], we confirmed normality of the time series used in the wavelet coherency analyses (using Lilliefors test).

3. Results and Discussion

3.1. Climate Signals in the OWDA

Correlations between winter (January–March; JFM) and spring (April–June; AMJ) precipitation and the tree ring reconstructed JJA scPDSI are uniformly positive across the basin (Figure 2). The strongest correlations with JFM precipitation are localized in Spain and Morocco in the western Mediterranean and the Levant region in the eastern basin. The AMJ precipitation correlations are more uniform and strongly positive across nearly the entire Mediterranean, suggesting that the summer (JJA) season soil moisture variability,

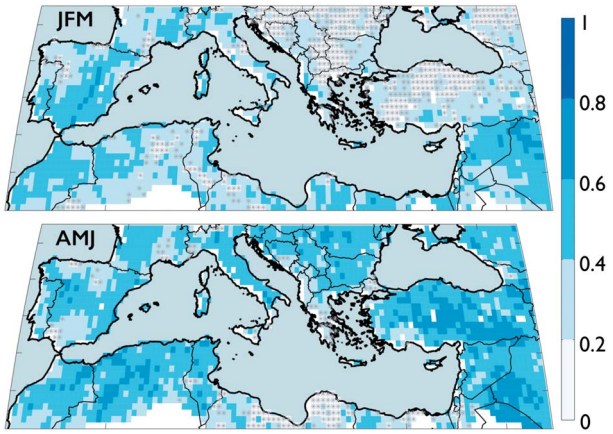

Figure 2. Point-by-point Spearman's rank correlation coefficients between CRU 3.21 precipitation totals (JFM and AMJ) and OWDA summer season (JJA) scPDSI. Correlations are calculated over the period 1950–2012 C.E. Regions of insignificant correlation ($p > 0.05$) are masked by grey asterisks.

reflected in the OWDA and the underlying tree growth, is driven primarily by spring precipitation [cf. *Touchan et al.*, 2011, 2014a].

Climate mode correlations with the CRU precipitation data or the OWDA scPDSI (Figure 3) are consistent in sign but generally stronger in the precipitation data. The weaker OWDA scPDSI correlations are expected for at least two reasons. First, these climate modes reflect shifts in atmospheric circulation that have a direct impact on precipitation by modulating, for example, storm track positions and moisture convergence. Circulation impacts on the scPDSI will be by definition more indirect, as the scPDSI is computed based on the anomalies of a variety of variables that influence soil moisture. And, as mentioned previously, through year 1978 the scPDSI is reconstructed as a scaled linear function of the underlying tree ring proxies, which imparts additional uncertainties on the estimates of scPDSI.

The influence of the NAO is strongest in winter and early spring (January–April). Positive phases of the NAO cause drying across the northern reaches of the Mediterranean Basin, from Spain and Morocco across to the Balkans and western Turkey, while favoring wetter conditions in coastal regions of Libya, Egypt, and the Levant. Consistent with both the instrumental observations [e.g., *Lamb et al.*, 1997; *Knippertz et al.*, 2003] and

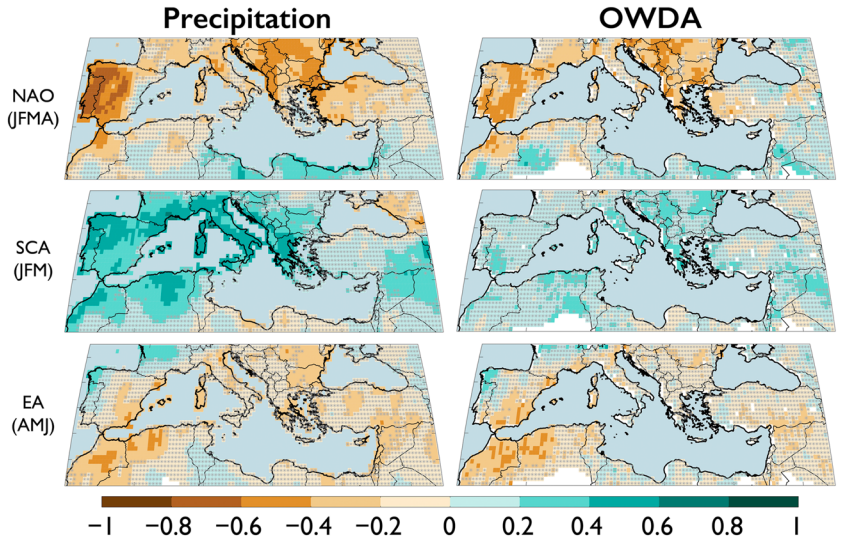

Figure 3. Spearman's rank correlation coefficients between the teleconnection indices (NAO, SCA, and EA) and (left column) simultaneous season CRU 3.21 precipitation totals and (right column) OWDA summer season scPDSI. Correlations are calculated over the period 1950–2012 C.E. Regions of insignificant correlation ($p > 0.05$) are masked by grey asterisks.

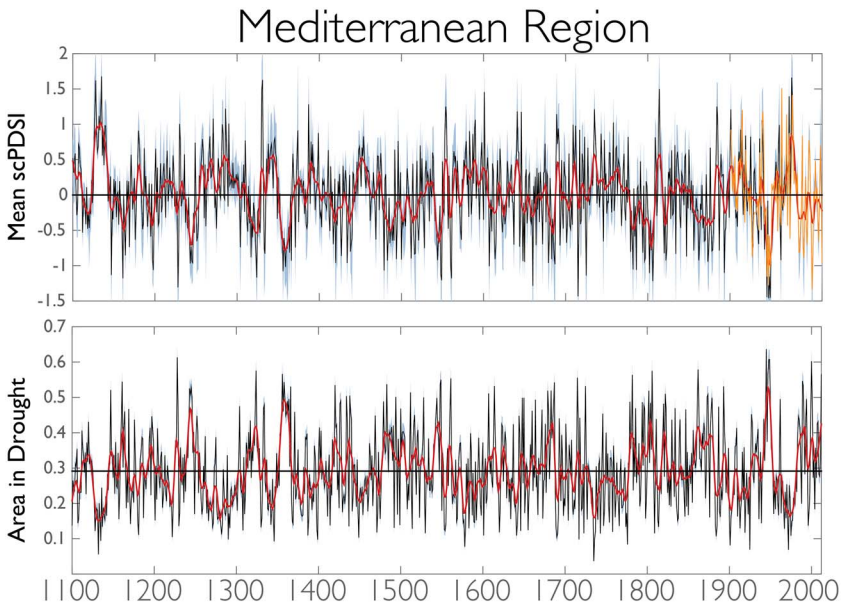

Figure 4. (top) Area average scPDSI for the entire Mediterranean domain in the OWDA (30°N–47°N, 10°W–45°E) and (bottom) percent land area in drought (scPDSI ≤ -1) from 1100 to 2012 C.E. Red curves are smoothed versions of the time series using a 10 year loess smooth. In Figure 4 (top), regional average scPDSI calculated from the instrumental target data set for the OWDA reconstruction is overlain in orange. The horizontal line in Figure 4 (bottom) is the long-term average fractional area in drought from 1100 to 2012 C.E. (29%). Grey-blue shading indicates the 95th confidence intervals, estimated using a BCa bootstrap.

the underlying controls on tree growth [*Touchan et al.*, 2008a, 2008b, 2011; *Panayotov et al.*, 2010], the influence of the NAO in the OWDA is strongest in the far western part of the domain and the Balkans. The largest influence of the SCA pattern is during the winter (JFM), with positive phases increasing moisture across most of the basin. The SCA correlation with the OWDA is substantially weaker, consistent with previous analyses (Figure 2) demonstrating the much stronger connection between the OWDA and spring, rather than winter, precipitation. Unlike the previous two modes, the influence of the EA is highest during the spring (AMJ), causing widespread drying across the basin with, notably, similar magnitude correlations with both precipitation and scPDSI.

The results from our teleconnection analyses are similar to previous studies quantifying connections between these climate modes and drought variability in the region. For example, *Sousa et al.* [2011] found comparable patterns of significant correlation between PDSI and the NAO. Their correlations with the SCA and EA are similar in sign, though with larger magnitudes and greater significance than in our analyses, possibly because they focused on different seasonal composites. Other comparisons between the NAO and precipitation over the Mediterranean are also similar [*Cullen and deMenocal*, 2000; *Roberts et al.*, 2012; *Xoplaki et al.*, 2004], showing a broad pattern of significant negative correlations across Southern Europe and out of phase anomalies over coastal Africa in the eastern part of the basin.

3.2. Drought Variability in the OWDA

Figure 4 shows OWDA scPDSI averaged over the Mediterranean domain and the fraction of the land area in drought conditions (scPDSI ≤ -1) each year from 1100 to 2012. Interannual variability (standard deviation) in the scPDSI is 0.54 standardized PDSI units, and, on average, 29% of the basin experiences drought conditions in any given year. Several periods of persistent, pan-Mediterranean drought are apparent in the record, including in the 1100s, 1200s, and 1300s. There is also a particularly strong pluvial event in the early 1100s. Noticeably absent, however, are any extended multidecadal (30 year or longer) "megadroughts," a characteristic feature of North American drought variability during the Medieval Climate Anomaly (approximately before 1300 C.E.) [e.g., *Cook et al.*, 2010a] and previously inferred from Moroccan tree rings [*Esper et al.*, 2007].

The spatial patterns of five periods of widespread drought (and one pluvial) are shown in Figure 5. A nearly two decade long pluvial occurred from 1125 to 1142 C.E., with sustained wet conditions in modern day Spain, Morocco, Algeria, Tunisia, Italy, the Balkans, and Turkey. This event occurred at the same time as an extended

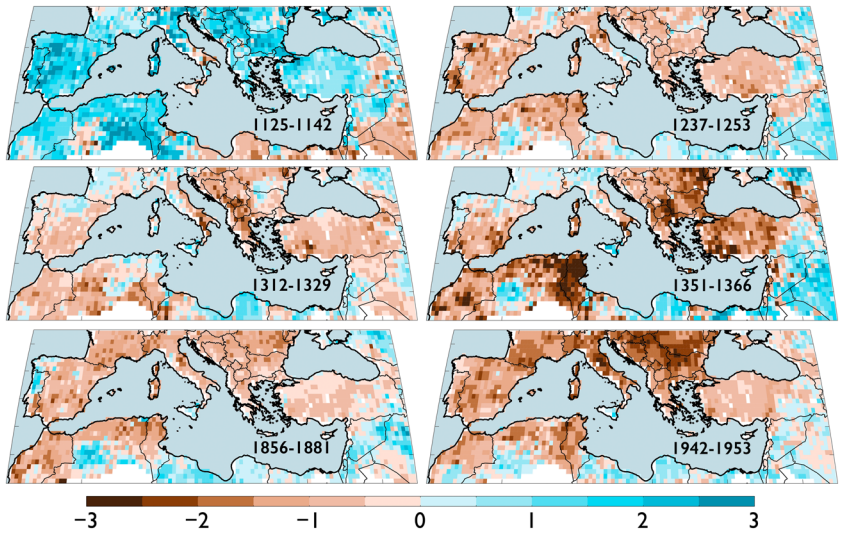

Figure 5. Multiyear average scPDSI for different pan-basin drought and pluvial events in the OWDA.

period (1118–1179 C.E.) of low flows in the Upper Colorado River Basin in North America (the most persistent dry period in that region over the last millennium) [*Meko et al.*, 2007], severe drought in the Sacramento River Basin [*Meko et al.*, 2012], and widespread drought across most of North America [*Cook et al.*, 2014a]. This synchrony is suggestive of a possible large-scale persistent anomaly in atmospheric circulation across the Atlantic, possibly related to shifts in Atlantic sea surface temperatures [*Hu and Feng*, 2012]. For the moment, however, such a relationship is speculative, requiring additional data to determine whether this co-occurrence is random or reflective of some real underlying dynamics. With Common Era drought atlases now available across all three continents of the Northern Hemisphere [*Cook et al.*, 2010a, 2010b, 2015], there may be new opportunities to investigate such a question in more detail.

Among the five highlighted persistent drought events (Figure 5), there is a tendency for simultaneous drought in the extreme western (Spain, Morocco, Algeria, and Tunisia) and eastern (Balkans, Greece, and Turkey) ends of the basin. This suggests a degree of spatial coherency and synchrony during major drought events in the basin. This is further confirmed by compositing the most widespread drought years in the Mediterranean, years when scPDSI values ≤ -1.0 cover at least 40% or 50% of the basin (Figure 6). Severe droughts occur synchronously at the opposite ends of the basin. Additionally, Figures 5 and 6 also show evidence for antiphasing behavior in the eastern end of the basin, where there is a tendency for Libya, Egypt, and the southern Levant to be wet or near normal when Greece and Anatolia are in drought. This meridional dipole structure bears some resemblance to the NAO correlation patterns with precipitation and scPDSI discussed previously (Figure 3).

These spatial patterns of variability have been documented in other studies of Mediterranean drought variability. For example, *Xoplaki et al.* [2004] previously noted north-south antiphasing in hydroclimate variability over the eastern Mediterranean and a tendency for zonally widespread drought events across the basin. These observations of spatial coherence are, however, contrary to previous analyses of other proxy records in the region, which have suggested instead a tendency for an antiphased dipole in hydroclimate variability between these two regions [*Roberts et al.*, 2012]. Whether these differences are due to intrinsic qualities of the proxies themselves or differing interpretations of the underlying data is still unclear.

Independent reconstructions of Mediterranean climate over the Common Era are available from a variety of proxies, including lake sediments, speleothems, and historical records [*Luterbacher et al.*, 2012]. Comparisons between these records and the OWDA, however, are difficult for several reasons, including temporal resolution and time uncertainty, spatial coverage, frequency biases, the reconstruction methodologies used, and the variables targeted for reconstruction (e.g., lake levels, precipitation, and raw isotope time series). The review by *Luterbacher et al.* [2012] highlights several centennial-scale periods of enhanced aridity or wetness in the Mediterranean during the Common Era from various different proxy reconstructions. Some of these records are at least qualitatively comparable to the OWDA. For example, the carbon isotope record from Uzuntarla

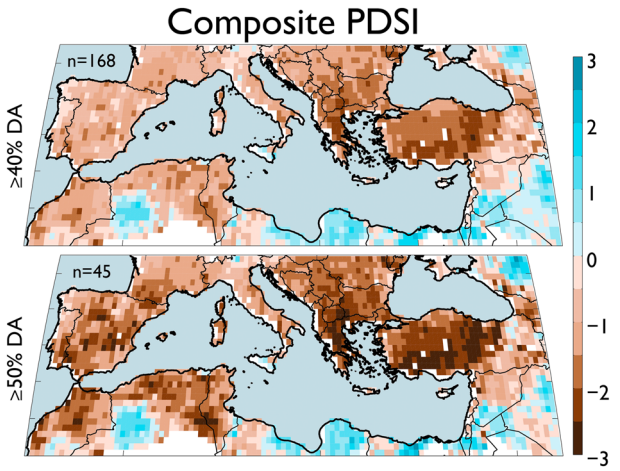

Figure 6. Composite average scPDSI for years in the OWDA with drought area (DA; scPDSI ≤ -1) exceeding 40% ($n=168$ years) and 50% ($n=45$ years) of the total land area in the Mediterranean domain.

Cave [*Fleitmann et al.*, 2009], in northwestern Turkey, identifies a wet period in the 1100s followed by a drought period in the 1200s, consistent with the variability identified in the OWDA (Figure 5).

Cook et al. [2015] provide several comparisons with previous records relevant for the Mediterranean region. The OWDA scPDSI is positively correlated with the historical precipitation reconstruction of *Pauling et al.* [2006] over the western Mediterranean (southern Spain, Morocco, Algeria, and Tunisia), Greece and the Balkans, and Anatolia [*Cook et al.*, 2015, Supplemental Figure 12]. The OWDA also identifies eight major historically documented droughts [*White*, 2006] that occurred during the Ottoman Empire in the late 1500s and early 1600s [*Cook et al.*, 2015, Supplemental Figure 17].

3.3. Spatial Synchrony

To further investigate the tendency for zonally synchronous hydroclimate variability across the basin, and meridional antiphasing in the eastern basin, we averaged scPDSI from the OWDA over three regions: the western Mediterranean (WestMED; 32°N–42°N, 10°W–0°E), the eastern Mediterranean (EastMED; 36°N–41°N, 20°E–37°E), and an area encompassing coastal Egypt, the southern Levant, and other areas of the Middle East (MidEast; 30°N–34°N, 33°E–47°E). The first two areas (WestMED and EastMED) correspond to approximately the same regions used in the analysis of *Roberts et al.* [2012]. Our MidEast box corresponds generally to the area of out-of-phase anomalies in Figures 5 and 6.

Point-by-point correlations (Figure 7) between these three indices and the OWDA are strongly positive at the local level, as expected, decaying in magnitude outside of the averaging regions. For WestMED the correlations remain mostly positive, or near zero, across the entire basin. EastMED, however, shows strong negative correlations over Libya, Egypt, and the Levant, while MidEast is negatively correlated with a large region surrounding the Black Sea. As with the drought composites (previous section), these results again suggest a strong tendency for meridional antiphasing in hydroclimate in the eastern Mediterranean Basin, with a pattern similar to what would be expected due to precipitation responses to variations in the NAO. Results are similar when the correlations are calculated on single-century subsets (1101–1200 C.E., 1201–1300 C.E., etc.) of the full data range (not shown), suggesting that the correlations across regions have been relatively stationary over time.

We further investigate the nature and strength of drought variability across these regions through various spectral coherency analyses. The spectra of the WestMED and EastMED time series show significant power at interannual and decadal to multidecadal frequencies (Figure 8). Both regions have significant peaks at about 3–4 years, with EastMED additionally peaking at decadal frequencies and WestMED significant across a broader range of multidecadal bands. The two regions also overlap in their power at around 70 years, though EastMED is only marginally significant at the 90th percentile. A coherency spectra analysis between the two regional indices demonstrates highly significant coherence between the two regions on interannual and decadal timescales (Figure 9). Notably, there is also a broad band of coherence between the two regions at multidecadal and centennial timescales (30 to 130 years), despite no significant spectral peaks at wavelengths

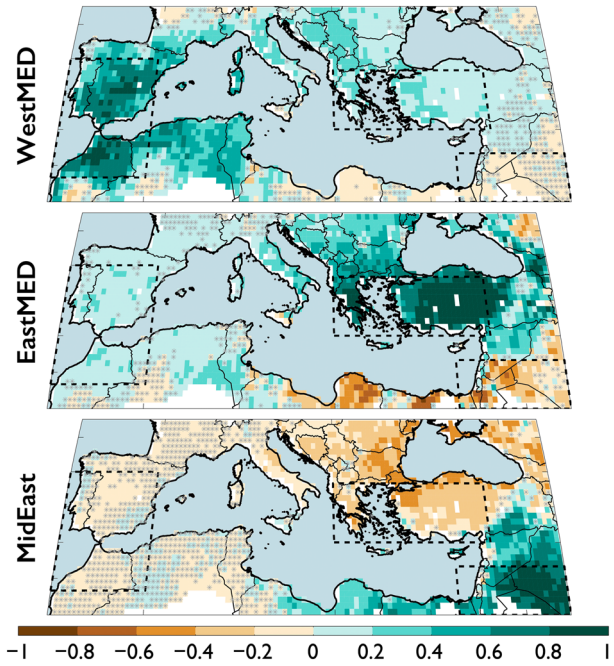

Figure 7. Point-by-point Spearman's rank correlations (1100–2012) between OWDA scPDSI and the western Mediterranean (WestMED; 32°N–42°N, 10°W–0°), eastern Mediterranean (EastMED; 36°N–41°N, 20°E–37°E), and Middle East (MidEast; 30°N–34°N, 33°E–47°E) regional average scPDSI time series. Regions of insignificant correlation ($p > 0.05$) are masked by grey asterisks.

longer than ~75 years in either WestMED or EastMED. This may be due to overlaps in shared frequencies: both series have peaks at around 70–75 years, approximately the first harmonic of the 130 year coherence in the coherency spectra. An analysis of the relative phasing for these spectral bands (not shown) indicates that the null hypothesis (i.e., WestMED and EastMED are in phase) cannot be rejected at the $p \leq 0.05$ significance level.

These results are further confirmed through a cross-wavelet coherency analysis (Figure 10), which shows that EastMED and WestMED share significant ($p \leq 0.05$) in-phase variance (i.e., black arrows point to the right) in decadal to centennial frequency bands across the record. Further, EastMED and MidEast have significant coherence at interannual to multidecadal frequencies but are largely 180° out of phase (i.e., blacks arrows are primarily pointing to 90° to the left). These results indicate that over most of the last millennium there is a reasonably strong tendency for in-phase drought in the zonal direction across the Mediterranean and out-of-phase variability in the eastern Mediterranean. Interestingly, given the association between the North Atlantic and western Mediterranean drought variability (Figure 3), there is no suggestion from the OWDA

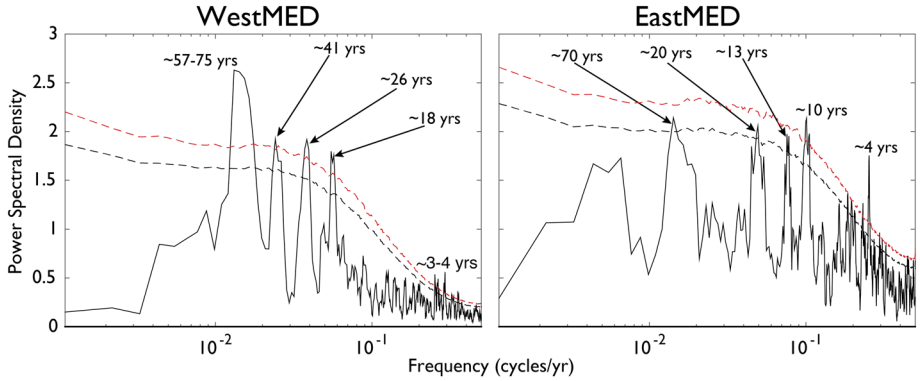

Figure 8. Power spectral density (multitaper method, three tapers) for the WestMED and EastMED regional average scPDSI series. Red and black dashed lines are the 95th and 90th percentile confidence limits, respectively, estimated from 10,000 AR(1) series generated from the original time series.

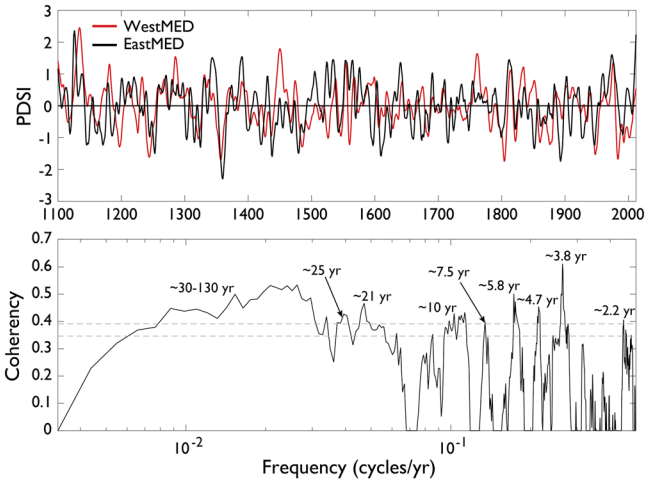

Figure 9. (top) Smoothed versions (10 year loess smooth) of the WestMED and EastMED time series and (bottom) the coherency spectra between unsmoothed versions of the two time series. Numbers in Figure 9 (bottom) highlight regions of significant coherency.

(Figure 9) that the NAO was in a persistent positive phase during the Medieval era. This is in contrast with conclusions from *Esper et al.* [2007] and *Trouet et al.* [2009] but is consistent with other regional climate reconstructions [*Touchan et al.*, 2008a, 2011] and in agreement with a recent multiproxy reconstruction of the NAO by *Ortega et al.* [2015].

3.4. Recent Droughts

Recent decades have witnessed persistent, multiyear droughts in the Mediterranean that have spurred speculation that warming-induced drying trends may have begun to emerge. In the OWDA, these droughts are not coherent across the Mediterranean Basin but are instead highly localized in the WestMED region, Greece (36°N–43°N, 19°E–26°), and the Levant (30°N–37°N, 33°E–40°E) (Figure 11). Both WestMED [*Touchan et al.*, 2008a, 2011] and Greece experienced significant droughts in the 1980s and 1990s that have since ended. The driest period in the Levant began in 1998 and persists through the end of the data set. Here we attempt to place these most recent drought events within the context of OWDA drought variability for the last 900 years (Figure 12).

Over the last 30 years (1980–2012), we identify major periods of persistent drought in all three of these regions: 1980–2009 (WestMED), 1984–2002 (Greece), and 1998–2012 (Levant) (Figure 13, black dots). We then calculated the mean scPDSI for moving windows of the same length in each regional time series.

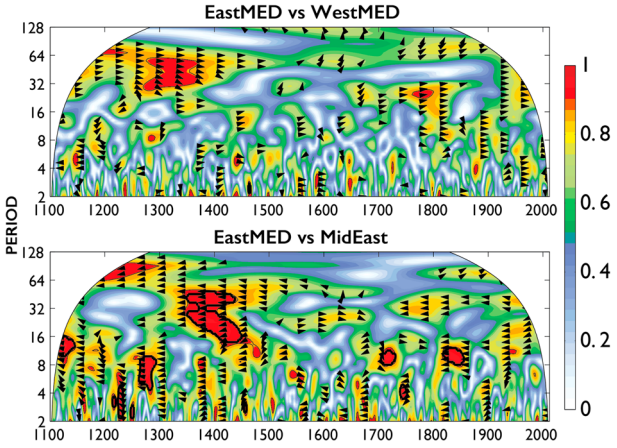

Figure 10. Squared wavelet coherence for (top) EastMED versus WestMED and (bottom) EastMED versus MidEast. Black arrows indicate where the two time series have significant ($p \leq 0.05$) shared variance. Relative phasing is indicated by the direction of the arrows; right pointing arrows indicate that series are in phase, and left pointing are 180° out of phase.

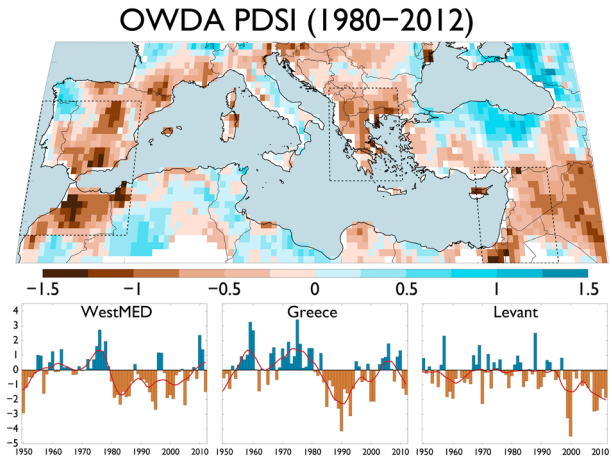

Figure 11. (top) Multiyear average scPDSI for 1980–2012 with regions of recent and persistent drought outlined in dashed black lines: WestMED (32°N–42°N, 10°W–0°), Greece (36°N–43°N, 19°E–26°), and the Levant (30°N–37°N, 33°E–40°E). (bottom) Also shown are the regional average scPDSI time series from these regions for 1950–2012 (red line is a 10 year loess smoother).

The interquartile range (IQR) of these moving window mean scPDSI values is shown in the grey bars in Figure 13, and the values for the driest windows prior to the most recent drought are shown by the grey dots (Figure 13). For the most recent droughts and the driest previous window, we estimate uncertainties using a resampling procedure where we randomly draw years from each window with replacement, recalculating the mean scPDSI for these intervals 10,000 times. The whiskers in Figure 13 represent the 25th and 75th percentiles of these 10,000 resampled means.

In general agreement with *Touchan et al.* [2008a], the recent persistent droughts in WestMED and Greece qualify as the most severe on the record back to 1100. In both regions, however, there is substantial overlap in the estimated uncertainties, and the recent droughts are not significantly drier (Student's *t* test, $p > 0.10$) than the

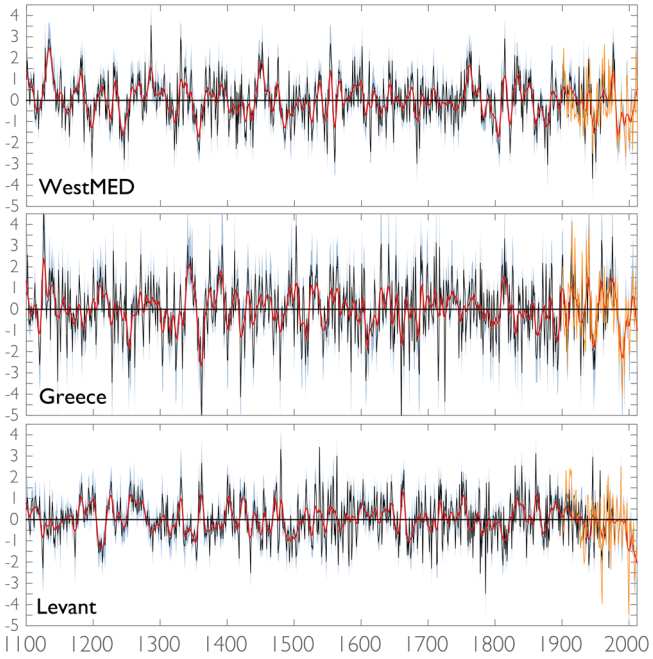

Figure 12. Recentered (zero mean from 1100 to 2012 C.E.) time series for WestMED, Greece, and the Levant region. Red lines represent smoothed versions using a 10 year loess smoother. Grey-blue shading indicates the 95th confidence intervals, estimated using a BCa bootstrap. In each panel, regional average scPDSI calculated from the instrumental target data set for the reconstructions is overlain in orange.

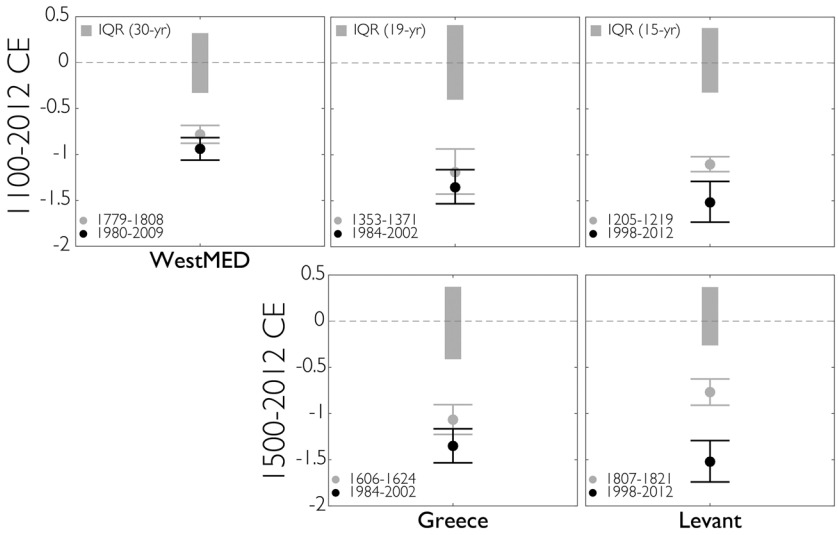

Figure 13. (top row) Comparisons between multiyear average, recentered scPDSI during recent decades (black dots), and the driest previous periods of the same length in the OWDA from 1100 to 2012 C.E. (grey dots). Grey bars are the interquartile range (IQR) of mean PDSI values for all moving windows of the same length in each region. Whiskers are the 25th and 75th confidence limits for the dry events, estimated from 10,000 resamplings with replacement from scPDSI values during these intervals. (bottom row) Same as Figure 13 (top row) but restricting the analysis to 1500–2012 C.E., when there is increased proxy availability in regions like the Levant.

previous driest windows. From this, we conclude that, while severe, recent droughts in the WestMED region and Greece do not significantly deviate from the range of natural drought variability over the last 900 years.

The magnitude of the recent Levant drought exceeds the magnitude of the driest previous interval in the region. In the Levant, mean scPDSI for 1998–2012 is −1.52, compared to −1.1 for 1205–1219, with nonoverlapping confidence limits between the two events. Despite this separation, 1998–2012 is not significantly drier than the previous driest period (one-sided Student's t test, $p = 0.13$). This is likely due to the leveraging of the mean scPDSI for 1998–2012 by several extremely dry years: 1999 (scPDSI = −3.25), 2000 (scPDSI = −4.49, the driest single year in this region back to 1100), 2008 (scPDSI = −2.80), and 2012 (scPDSI = −2.72). In 89% of our simulations, however, the resampled mean scPDSI for 1998–2012 was drier than the resampled mean for the previous driest interval, 1205–1219.

Because of concerns regarding proxy availability in the early part of our record, we repeat our analysis comparing recent droughts to variability from 1500 to 2012 C.E. (Figure 13, bottom row), when proxy availability is much better, especially in the Levant region (Figure 1). In the case of WestMED, the driest previous window of the last 900 years occurs after 1500 (1779–1808), and so this analysis is not repeated. For Greece, the most recent drought is still not significantly drier than the driest comparable period after 1500 (1606–1624). For the Levant, however, the most recent drought is significantly drier (one-sided Student's t test, $p = 0.04$) than the driest interval of the last 500 years (1807–1821). This is confirmed by the resampling, where 1998–2012 is drier than 1807–1821 in 98% of our simulations. From these results, we conclude that 1998–2012 in the Levant was likely the driest 15 year period of the last 900 years and very likely the driest of the last 500.

4. Conclusions

Paleoclimate reconstructions provide better sampling of the full range and spectrum of natural variability in the climate system, information that is often not adequately captured in the relatively short instrumental record. This knowledge is especially critical for improving our understanding of low-frequency variability (decadal to multidecadal), a necessary step for evaluating the extent to which anthropogenic forcing may be influencing recent climate events. The OWDA is the latest such reconstruction, providing an annually resolved spatiotemporal view of droughts and pluvials across Europe and the Mediterranean Basin.

We find significant decadal to multidecadal variability in hydroclimate across the Mediterranean in the OWDA, with significant coherence between the western and eastern basin centers on multidecadal to centennial timescales and meridional antiphasing in the eastern Mediterranean Basin. The dynamics driving these

patterns are still uncertain, but the NAO or processes linked to the North Atlantic are likely to be a major contributors [*Hurrell and Loon*, 1997; *Eshel and Farrell*, 2000]. The NAO mode is negatively correlated with precipitation, and scPDSI across most of the basin (Figure 2) and at the decadal scale is associated with same-sign wet season (boreal winter) precipitation anomalies from Morocco and the Iberian Peninsula through western and central Anatolia, with opposing anomalies in the Levant [*Mariotti et al.*, 2002; *Xoplaki et al.*, 2004]. And while there is a zonal dipole in the Mediterranean tree ring response to precipitation, with a stronger winter response to the west and an increasing spring-summer signal in the east [*Touchan et al.*, 2014a, 2014b], at decadal timescales at least the summer scPDSI does appear to reflect the broad-scale forcing of precipitation anomalies associated with the NAO. This creates a basin-wide coherence between northwestern Africa, the Balkans, and western Anatolia (Figure 9) and opposite sign anomalies in the Levant during major Mediterranean drought and pluvial events (Figures 5–7). However, work is needed to better reconcile our results with other reconstructions that offer alternative interpretations of hydroclimate variability across the basin, such as the east-west seesaw in the study of *Roberts et al.* [2012].

Interestingly, this coherent decadal pattern is somewhat different than that observed for recent scPDSI trends (Figures 11–13), with the western Mediterranean and the Levant experiencing more substantial drying trends and with mixed signs over Anatolia. This suggests that North Atlantic ocean-atmosphere variability alone is unlikely to account for recent drought trends and supports interpretations that greenhouse gas forcing has an important influence [*Kelley et al.*, 2012; *Seager et al.*, 2014; *Kelley et al.*, 2015]. Although some climate model simulations suggest that recent NAO trends are outside the range of natural variability [*Osborn*, 2004; *Kuzmina et al.*, 2005], long control simulations can demonstrate unforced NAO variability similar to that seen in recent decades [*Semenov et al.*, 2008]. Drying in the Levant is also likely influenced by recent trends toward a more positive EA pattern [*Krichak et al.*, 2002; *Krichak and Alpert*, 2005; *Lim*, 2014].

Our findings indicate that recent droughts in the western Mediterranean and Greece are not yet outside the range of the last 900 years of natural variability, despite the influence of greenhouse gas forcing. For the Levant, however, we estimate that 1998–2012 in the OWDA is likely (89% likelihood) the driest 15 year period in the region since the twelfth century, with even greater confidence (98% likelihood) that it is the driest back to 1500 C.E. Our analysis does not directly inform our understanding of the magnitude of anthropogenic influence on recent droughts in the region. We can also only analyze such an event in the OWDA from the perspective of a singular drought metric (scPDSI) that may have different sensitivities compared to other variables (e.g., precipitation and streamflow). The results from our Levant analysis do, however, suggest that recent dry extremes are exceptional relative to natural variability during the last millennium. This offers some independent support for recent studies concluding that anthropogenic climate change has had a significant influence [e.g., *Kelley et al.*, 2015].

Drought conditions in this region are likely to be further exacerbated in the future with climate change [e.g., *Cook et al.*, 2014b; *Dubrovský et al.*, 2014], amplifying the potential for sociopolitical and economic disruption [e.g., *Gleick*, 2014; *Kelley et al.*, 2015]. Dealing with the consequences of aridification for societies and ecosystems in the region will require a multidisciplinary research, management, and policy approach [*Sohl and van Ginkel*, 2014]. To that end, paleoclimate field reconstructions, like the OWDA, can provide valuable information on longer-term natural climate variability and aid in the interpretation of recent events and possible climate change contributions.

Acknowledgments
Funding for Anchukaitis, Meko, and Touchan was provided by grants from the NSF Paleo Perspectives on Climate Change (P2C2) program AGS-1103450, AGS-1103314, and AGS-1341066, with additional support from the NSF awards AGS-0317288 (Earth System History), AGS-0758486, and AGS-0075956. Funding for the OWDA provided to E.R. Cook was by NOAA grant NA10OAR4310123. E.R. Cook and Anchukaitis are also supported by NSF AGS-1501856 and AGS-1502224. Support for B.I. Cook was provided by NASA. The Old World Drought Atlas is archived and freely available from the National Centers for Environmental Information (NCEI) at the National Oceanic and Atmospheric Administration (https://www.ncdc.noaa.gov/data-access/paleoclimatology-data). This is Lamont contribution 7977.

References

Akkemik, U., and A. Aras (2005), Reconstruction (1689–1994 AD) of April–August precipitation in the southern part of central Turkey, *Int. J. Climatol.*, *25*(4), 537–548, doi:10.1002/joc.1145.

Andreu, L., E. Gutiérrez, M. Macias, M. Ribas, O. Bosch, and J. J. Camarero (2007), Climate increases regional tree-growth variability in Iberian pine forests, *Global Change Biol.*, *13*(4), 804–815, doi:10.1111/j.1365-2486.2007.01322.x.

Barnston, A. G., and R. E. Livezey (1987), Classification, seasonality and persistence of low-frequency atmospheric circulation patterns, *Mon. Weather Rev.*, *115*(6), 1083–1126, doi:10.1175/1520-0493(1987)115<1083:CSAPOL>2.0.CO;2.

Brewer, S., S. Alleaume, J. Guiot, and A. Nicault (2007), Historical droughts in Mediterranean regions during the last 500 years: A data/model approach, *Clim. Past*, *3*(2), 355–366, doi:10.5194/cp-3-355-2007.

Bueh, C., and H. Nakamura (2007), Scandinavian pattern and its climatic impact, *Q. J. R. Meteorol. Soc.*, *133*(629), 2117–2131, doi:10.1002/qj.173.

Büntgen, U., D. Frank, V. Trouet, and J. Esper (2010), Diverse climate sensitivity of Mediterranean tree-ring width and density, *Trees*, *24*(2), 261–273, doi:10.1007/s00468-009-0396-y.

Carro-Calvo, L., S. Salcedo-Sanz, and J. Luterbacher (2013), Neural computation in paleoclimatology: General methodology and a case study, *Neurocomputing*, *113*, 262–268, doi:10.1016/j.neucom.2012.12.045.

Chave, A. D., D. J. Thomson, and M. E. Ander (1987), On the robust estimation of power spectra, coherences, and transfer functions, *J. Geophys. Res.*, *92*(B1), 633–648, doi:10.1029/JB092ib01p00633.
Chbouki, N., C. W. Stockton, and D. Myers (1995), Spatio-temporal patterns of drought in Morocco, *Int. J. Climatol.*, *15*, 187–205, doi:10.1002/joc.3370150205.
Cleveland, W. S., and S. J. Devlin (1988), Locally weighted regression: An approach to regression analysis by local fitting, *J. Am. Stat. Assoc.*, *83*(403), 596–610, doi:10.2307/2289282.
Collins, M., et al. (2013), Long-term climate change: Projections, commitments and irreversibility, in *Climate Change 2013: The Physical Science Basis. Contribution of Working Group I to the Fifth Assessment Report of the Intergovernmental Panel on Climate Change*, edited by T. Stocker et al., pp. 1029–1136, Cambridge Univ. Press, Cambridge, U. K., and New York, doi:10.1017/CBO9781107415324.024.
Cook, B. I., J. E. Smerdon, R. Seager, and E. R. Cook (2014a), Pan-continental droughts in North America over the last millennium, *J. Clim.*, *27*(1), 383–397, doi:10.1175/JCLI-D-13-00100.1.
Cook, B. I., J. E. Smerdon, R. Seager, and S. Coats (2014b), Global warming and 21st century drying, *Clim. Dyn.*, *43*(9–10), 2607–2627, doi:10.1007/s00382-014-2075-y.
Cook, E. R., D. M. Meko, D. W. Stahle, and M. K. Cleaveland (1999), Drought reconstructions for the continental United States, *J. Clim.*, *12*(4), 1145–1162, doi:10.1175/1520-0442(1999)012<1145:DRFTCU>2.0.CO;2.
Cook, E. R., R. Seager, R. R. Heim Jr., R. S. Vose, C. Herweijer, and C. Woodhouse (2010a), Megadroughts in North America: Placing IPCC projections of hydroclimatic change in a long-term palaeoclimate context, *J. Quat. Sci.*, *25*(1), 48–61, doi:10.1002/jqs.1303.
Cook, E. R., K. J. Anchukaitis, B. M. Buckley, R. D. D'Arrigo, G. C. Jacoby, and W. E. Wright (2010b), Asian monsoon failure and megadrought during the last millennium, *Science*, *328*(5977), 486–489, doi:10.1126/science.1185188.
Cook, E. R., P. J. Krusic, K. J. Anchukaitis, B. M. Buckley, T. Nakatsuka, and M. Sano (2013), Tree-ring reconstructed summer temperature anomalies for temperate East Asia since 800 C.E, *Clim. Dyn.*, *41*(11–12), 2957–2972, doi:10.1007/s00382-012-1611-x.
Cook, E. R., et al. (2015), Old World megadroughts and pluvials during the Common Era, *Sci. Adv.*, *1*(10), e1500561, doi:10.1126/sciadv.1500561.
Cullen, H. M., and P. B. deMenocal (2000), North Atlantic influence on Tigris–Euphrates streamflow, *Int. J. Climatol.*, *20*(8), 853–863, doi:10.1002/1097-0088(20000630)20:8<853::AID-JOC497>3.0.CO;2-M.
Czaja, A., and J. Marshall (2001), Observations of atmosphere-ocean coupling in the North Atlantic, *Q. J. R. Meteorol. Soc.*, *127*(576), 1893–1916, doi:10.1002/qj.49712757603.
Dubrovský, M., M. Hayes, P. Duce, M. Trnka, M. Svoboda, and P. Zara (2014), Multi-GCM projections of future drought and climate variability indicators for the Mediterranean region, *Reg. Environ. Change*, *14*(5), 1907–1919, doi:10.1007/s10113-013-0562-z.
Efron, B. (1987), Better bootstrap confidence intervals, *J. Am. Stat. Assoc.*, *82*(397), 171–185.
Eshel, G., and B. F. Farrell (2000), Mechanisms of eastern Mediterranean rainfall variability, *J. Atmos. Sci.*, *57*(19), 3219–3232.
Esper, J., D. Frank, U. Büntgen, A. Verstege, J. Luterbacher, and E. Xoplaki (2007), Long-term drought severity variations in Morocco, *Geophys. Res. Lett.*, *34*, L17702, doi:10.1029/2007GL030844.
Fleitmann, D., et al. (2009), Timing and climatic impact of Greenland interstadials recorded in stalagmites from northern Turkey, *Geophys. Res. Lett.*, *36*, L19707, doi:10.1029/2009GL040050.
García-Ruiz, J. M., J. I. López-Moreno, S. M. Vicente-Serrano, T. Lasanta-Martínez, and S. Beguería (2011), Mediterranean water resources in a global change scenario, *Earth Sci. Rev.*, *105*(3–4), 121–139, doi:10.1016/j.earscirev.2011.01.006.
Giorgi, F., and P. Lionello (2008), Climate change projections for the Mediterranean region, *Global Planet. Change*, *63*(2–3), 90–104, doi:10.1016/j.gloplacha.2007.09.005.
Gleick, P. H. (2014), Water, drought, climate change, and conflict in Syria, *Weather Clim. Soc.*, *6*(3), 331–340, doi:10.1175/WCAS-D-13-00059.1.
Glueck, M. F., and C. W. Stockton (2001), Reconstruction of the North Atlantic Oscillation, 1429–1983, *Int. J. Climatol.*, *21*, 1453–1465, doi:10.1002/joc.684.
Grinsted, A., J. C. Moore, and S. Jevrejeva (2004), Application of the cross wavelet transform and wavelet coherence to geophysical time series, *Nonlinear Processes Geophys.*, *11*, 561–566.
Guttman, N. B. (1998), Comparing the palmer drought index and the standardized precipitation index, *J. Am. Water Resour. Assoc.*, *34*, 113–121, doi:10.1111/j.1752-1688.1998.tb05964.x.
Harris, I., P. D. Jones, T. J. Osborn, and D. H. Lister (2014), Updated high-resolution grids of monthly climatic observations—The CRU TS3.10 Dataset, *Int. J. Climatol.*, *34*(3), 623–642, doi:10.1002/joc.3711.
Held, I. M., and B. J. Soden (2006), Robust responses of the hydrological cycle to global warming, *J. Clim.*, *19*(21), 5686–5699, doi:10.1175/JCLI3990.1.
Hoerling, M., J. Eischeid, J. Perlwitz, X. Quan, T. Zhang, and P. Pegion (2012), On the increased frequency of Mediterranean drought, *J. Clim.*, *25*(6), 2146–2161, doi:10.1175/JCLI-D-11-00296.1.
Hu, Q., and S. Feng (2012), AMO- and ENSO-driven summertime circulation and precipitation variations in North America, *J. Clim.*, *25*(19), 6477–6495, doi:10.1175/JCLI-D-11-00520.1.
Hurrell, J. W. (1995), Decadal trends in the North Atlantic Oscillation: Regional temperatures and precipitation, *Science*, *269*(5224), 676–679, doi:10.1126/science.269.5224.676.
Hurrell, J. W., and H. V. Loon (1997), Decadal variations in climate associated with the North Atlantic Oscillation, in *Climatic Change at High Elevation Sites*, edited by H. F. Diaz, M. Beniston, and R. S. Bradley, pp. 69–94, Springer, Netherlands, doi:10.1007/978-94-015-8905-5_4.
Huybers, P. (2004), Comments on "coupling of the hemispheres in observations and simulations of glacial climate change" by A. Schmittner, O. A. Saenko, And A. J. Weaver', *Quat. Sci. Rev.*, *23*(1–2), 207–210, doi:10.1016/j.quascirev.2003.08.001.
Iglesias, A., L. Garrote, F. Flores, and M. Moneo (2007), Challenges to manage the risk of water scarcity and climate change in the Mediterranean, *Water Resour. Manage.*, *21*(5), 775–788, doi:10.1007/s11269-006-9111-6.
Jex, C. N., A. Baker, J. M. Eden, W. J. Eastwood, I. J. Fairchild, M. J. Leng, L. Thomas, and H. J. Sloane (2011), A 500 yr speleothem-derived reconstruction of late autumn–winter precipitation, northeast Turkey, *Quat. Res.*, *75*(3), 399–405, doi:10.1016/j.yqres.2011.01.005.
Jones, M. D., C. N. Roberts, M. J. Leng, and M. Türkeś (2006), A high-resolution late Holocene lake isotope record from Turkey and links to North Atlantic and monsoon climate, *Geology*, *34*(5), 361–364, doi:10.1130/G22407.1.
Kelley, C., M. Ting, R. Seager, and Y. Kushnir (2012), The relative contributions of radiative forcing and internal climate variability to the late 20th Century winter drying of the Mediterranean region, *Clim. Dyn.*, *38*(9–10), 2001–2015, doi:10.1007/s00382-011-1221-z.
Kelley, C. P., S. Mohtadi, M. A. Cane, R. Seager, and Y. Kushnir (2015), Climate change in the Fertile Crescent and implications of the recent Syrian drought, *Proc. Natl. Acad. Sci. U.S.A.*, *112*(11), 3241–3246, doi:10.1073/pnas.1421533112.
Knippertz, P., M. Christoph, and P. Speth (2003), Long-term precipitation variability in Morocco and the link to the large-scale circulation in recent and future climates, *Meteorol. Atmos. Phys.*, *83*(1), 67–88, doi:10.1007/s00703-002-0561-y.

Köse, N., U. Akkemik, H. N. Dalfes, and M. S. Özeren (2011), Tree-ring reconstructions of May–June precipitation for western Anatolia, *Quat. Res.*, *75*(3), 438–450, doi:10.1016/j.yqres.2010.12.005.
Krichak, S., P. Kishcha, and P. Alpert (2002), Decadal trends of main Eurasian oscillations and the Eastern Mediterranean precipitation, *Theor. Appl. Climatol.*, *72*(3–4), 209–220.
Krichak, S. O., and P. Alpert (2005), Decadal trends in the east Atlantic–west Russia pattern and Mediterranean precipitation, *Int. J. Climatol.*, *25*(2), 183–192, doi:10.1002/joc.1124.
Kuzmina, S. I., L. Bengtsson, O. M. Johannessen, H. Drange, L. P. Bobylev, and M. W. Miles (2005), The North Atlantic Oscillation and greenhouse-gas forcing, *Geophys. Res. Lett.*, *32*, L04703, doi:10.1029/2004GL021064.
Lamb, P. J., M. E. Hamly, and D. H. Portis (1997), North Atlantic Oscillation, *Geo Observateur*, *7*, 103–113.
Lim, Y.-K. (2014), The East Atlantic/West Russia (EA/WR) teleconnection in the North Atlantic: Climate impact and relation to Rossby wave propagation, *Clim. Dyn.*, *44*, 3211–3222, doi:10.1007/s00382-014-2381-4.
Luterbacher, J., et al. (2012), A review of 2000 years of paleoclimatic evidence in the Mediterranean, in *The Climate of the Mediterranean Region*, edited by P. Lionello, pp. 87–185, Elsevier, Oxford, U. K., doi:10.1016/B978-0-12-416042-2.00002-1.
Mann, M. E., and J. M. Lees (1996), Robust estimation of background noise and signal detection in climatic time series, *Clim. Change*, *33*(3), 409–445, doi:10.1007/BF00142586.
Maraun, D., and J. Kurths (2004), Cross wavelet analysis: Significance testing and pitfalls, *Nonlinear Processes Geophys.*, *11*(4), 505–514, doi:10.5194/npg-11-505-2004.
Maraun, D., J. Kurths, and M. Holschneider (2007), Nonstationary Gaussian processes in wavelet domain: Synthesis, estimation, and significance testing, *Phys. Rev. E*, *75*, 016707, doi:10.1103/PhysRevE.75.016707.
Mariotti, A., M. V. Struglia, N. Zeng, and K. Lau (2002), The hydrological cycle in the Mediterranean region and implications for the water budget of the Mediterranean Sea, *J. Clim.*, *15*(13), 1674–1690, doi:10.1175/1520-0442(2002)015<1674:THCITM>2.0.CO;2.
Meko, D., C. Woodhouse, and K. Morino (2012), Dendrochronology and links to streamflow, *J. Hydrol.*, *412–413*, 200–209, doi:10.1016/j.jhydrol.2010.11.041.
Meko, D. M., C. A. Woodhouse, C. A. Baisan, T. Knight, J. J. Lukas, M. K. Hughes, and M. W. Salzer (2007), Medieval drought in the upper Colorado River Basin, *Geophys. Res. Lett.*, *34*(10), 10,705–10,709, doi:10.1029/2007GL029988.
Moreno, A., et al. (2012), The Medieval Climate Anomaly in the Iberian Peninsula reconstructed from marine and lake records, *Quat. Sci. Rev.*, *43*, 16–32, doi:10.1016/j.quascirev.2012.04.007.
Nicault, A., S. Alleaume, S. Brewer, M. Carrer, P. Nola, and J. Guiot (2008), Mediterranean drought fluctuation during the last 500 years based on tree-ring data, *Clim. Dyn.*, *31*(2–3), 227–245, doi:10.1007/s00382-007-0349-3.
Ortega, P., F. Lehner, D. Swingedouw, V. Masson-Delmotte, C. C. Raible, M. Casado, and P. Yiou (2015), A model-tested North Atlantic Oscillation reconstruction for the past millennium, *Nature*, *523*(7558), 71–74, doi:10.1038/nature14518.
Osborn, T. (2004), Simulating the winter North Atlantic Oscillation: The roles of internal variability and greenhouse gas forcing, *Clim. Dyn.*, *22*(6–7), 605–623, doi:10.1007/s00382-004-0405-1.
Palmer, W. C. (1965), Meteorological drought, *Tech. Rep.*, US Weather Bureau, Washington, D. C.
Panayotov, M., P. Bebi, V. Trouet, and S. Yurukov (2010), Climate signal in tree-ring chronologies of Pinus peuce and Pinus heldreichii from the Pirin Mountains in Bulgaria, *Trees*, *24*(3), 479–490, doi:10.1007/s00468-010-0416-y.
Pauling, A., J. Luterbacher, C. Casty, and H. Wanner (2006), Five hundred years of gridded high-resolution precipitation reconstructions over Europe and the connection to large-scale circulation, *Clim. Dyn.*, *26*(4), 387–405, doi:10.1007/s00382-005-0090-8.
Roberts, N., et al. (2012), Palaeolimnological evidence for an east–west climate see-saw in the Mediterranean since AD 900, *Global Planet. Change*, *84*, 23–34, doi:10.1016/j.gloplacha.2011.11.002.
Seager, R., N. Naik, and G. A. Vecchi (2010), Thermodynamic and dynamic mechanisms for large-scale changes in the hydrological cycle in response to global warming, *J. Clim.*, *23*(17), 4651–4668, doi:10.1175/2010JCLI3655.1.
Seager, R., H. Liu, N. Henderson, I. Simpson, C. Kelley, T. Shaw, Y. Kushnir, and M. Ting (2014), Causes of increasing aridification of the Mediterranean region in response to rising greenhouse gases, *J. Clim.*, *27*(12), 4655–4676, doi:10.1175/JCLI-D-13-00446.1.
Seim, A., K. Treydte, V. Trouet, D. Frank, P. Fonti, W. Tegel, M. Panayotov, L. Fernández-Donado, P. Krusic, and U. Büntgen (2015), Climate sensitivity of Mediterranean pine growth reveals distinct east-west dipole, *Int. J. Climatol.*, *35*, 2503–2513, doi:10.1002/joc.4137.
Semenov, V. A., M. Latif, J. H. Jungclaus, and W. Park (2008), Is the observed NAO variability during the instrumental record unusual?, *Geophys. Res. Lett.*, *35*, L11701, doi:10.1029/2008GL033273.
Sohl, M., and M. van Ginkel (2014), Drought preparedness and drought mitigation in the developing world's drylands, *Weather Clim. Extremes*, *3*, 62–66, doi:10.1016/j.wace.2014.03.003.
Sousa, P. M., R. M. Trigo, P. Aizpurua, R. Nieto, L. Gimeno, R. Garcia-Herrera, P. Lionello, and M. Maugeri (2011), Trends and extremes of drought indices throughout the 20th century in the Mediterranean, *Nat. Hazards Earth Syst. Sci.*, *11*(1), 33–51, doi:10.5194/nhess-11-33-2011.
Thomson, D. J. (1982), Spectrum estimation and harmonic analysis, *Proc. IEEE*, *70*, 1055–1096.
Touchan, R., G. M. Garfin, D. M. Meko, G. Funkhouser, N. Erkan, M. K. Hughes, and B. S. Wallin (2003), Preliminary reconstructions of spring precipitation in southwestern Turkey from tree-ring width, *Int. J. Climatol.*, *23*(2), 157–171, doi:10.1002/joc.850.
Touchan, R., E. Xoplaki, G. Funkhouser, J. Luterbacher, M. K. Hughes, N. Erkan, U. Akkemik, and J. Stephan (2005), Reconstructions of spring/summer precipitation for the Eastern Mediterranean from tree-ring widths and its connection to large-scale atmospheric circulation, *Clim. Dyn.*, *25*(1), 75–98, doi:10.1007/s00382-005-0016-5.
Touchan, R., K. J. Anchukaitis, D. M. Meko, S. Attalah, C. Baisan, and A. Aloui (2008a), Long term context for recent drought in northwestern Africa, *Geophys. Res. Lett.*, *35*, L13705, doi:10.1029/2008GL034264.
Touchan, R., D. Meko, and A. Aloui (2008b), Precipitation reconstruction for Northwestern Tunisia from tree rings, *J. Arid. Environ.*, *72*(10), 1887–1896, doi:10.1016/j.jaridenv.2008.05.010.
Touchan, R., K. J. Anchukaitis, D. M. Meko, M. Sabir, S. Attalah, and A. Aloui (2011), Spatiotemporal drought variability in northwestern Africa over the last nine centuries, *Clim. Dyn.*, *37*(1–2), 237–252, doi:10.1007/s00382-010-0804-4.
Touchan, R., K. J. Anchukaitis, V. V. Shishov, F. Sivrikaya, J. Attieh, M. Ketmen, J. Stephan, I. Mitsopoulos, A. Christou, and D. M. Meko (2014a), Spatial patterns of eastern Mediterranean climate influence on tree growth, *Holocene*, *24*(4), 381–392, doi:10.1177/0959683613518594.
Touchan, R., D. M. Meko, and K. J. Anchukaitis (2014b), Dendroclimatology in the Eastern Mediterranean, *Tree Ring Res.*, *70*(3), S61–S68, doi:10.3959/1536-1098-70.3.61.
Trouet, V., J. Esper, N. E. Graham, A. Baker, J. D. Scourse, and D. C. Frank (2009), Persistent positive North Atlantic Oscillation mode dominated the medieval climate anomaly, *Science*, *324*(5923), 78–80, doi:10.1126/science.1166349.
van der Schrier, G., J. Barichivich, K. R. Briffa, and P. D. Jones (2013), A scPDSI-based global data set of dry and wet spells for 1901–2009, *J. Geophys. Res. Atmos.*, *118*, 4025–4048, doi:10.1002/jgrd.50355.

Vicente-Serrano, S. M., S. Beguería, J. I. López-Moreno, M. Angulo, and A. El Kenawy (2010), A new global 0.5 gridded dataset (1901–2006) of a multiscalar drought index: Comparison with current drought index datasets based on the Palmer Drought Severity Index, *J. Hydrometeorol.*, *11*(4), 1033–1043, doi:10.1175/2010JHM1224.1.

Wassenburg, J. A., et al. (2013), Moroccan speleothem and tree ring records suggest a variable positive state of the North Atlantic Oscillation during the Medieval Warm Period, *Earth Planet. Sci. Lett.*, *375*, 291–302, doi:10.1016/j.epsl.2013.05.048.

White (Ed.), S. A. (2006), Climate change and crisis in Ottomon Turkey and the Balkans, 1590–1710, in *Proceedings of International Conference on Climate Change in the Middle East: Past, Present and Future, 20–23 Nov.*, pp. 391–409, Istanbul Tech. Univ., Istanbul, Turkey.

Xoplaki, E., J. González-Rouco, J. Luterbacher, and H. Wanner (2004), Wet season Mediterranean precipitation variability: Influence of large-scale dynamics and trends, *Clim. Dyn.*, *23*(1), 63–78, doi:10.1007/s00382-004-0422-0.

Xu, C.-Y., and V. P. Singh (2002), Cross comparison of empirical equations for calculating potential evapotranspiration with data from Switzerland, *Water Resour. Manage.*, *16*(3), 197–219, doi:10.1023/A:1020282515975.